Stimulation of Microtubule Aster Formation and Spindle Assembly by the Small GTPase Ran

Andrew Wilde and Yixian Zheng*

Ran, a small guanosine triphosphatase, is suggested to have additional functions beyond its well-characterized role in nuclear trafficking. Guanosine triphosphate–bound Ran, but not guanosine diphosphate–bound Ran, stimulated polymerization of astral microtubules from centrosomes assembled on *Xenopus* sperm. Moreover, a Ran allele with a mutation in the effector domain (RanL43E) induced the formation of microtubule asters and spindle assembly, in the absence of sperm nuclei, in a γTuRC (γ-tubulin ring complex)– and XMAP215 (*Xenopus* microtubule associated protein)–dependent manner. Therefore, Ran could be a key signaling molecule regulating microtubule polymerization during mitosis.

In animal cells, the transition from interphase to mitosis is accompanied by pronounced changes in cellular architecture. One of the biggest changes is the conversion of the interphase microtubule array into a highly dynamic mitotic spindle. This requires more than the presence of microtubule nucleating centers (called centrosomes in animal cells) and the conversion of cytosol into a mitotic state (*1*, *2*). Nuclear signals released into the cytoplasm upon nuclear envelope breakdown (NEB) influence the organization of the microtubule arrays. For example, premature rupture of the nuclear envelope in grasshopper spermatocytes during prophase causes the formation of a mitotic spindle next to the chromosomes (*3*). Chromosomes and nuclei themselves can initiate large microtubule asters from nearby centrosomes (*4*, *5*). Even in the absence of centrosomes, for example, during meiosis in female *Drosophila*, microtubule assembly is promoted near chromosomes (*6*). Chromosomes can also polarize existing microtubule arrays into a spindle-like structure in mitosis (*7*). Furthermore, artificial chromosomes tethered to beads stimulate mitotic spindle formation in the absence of centrosomes and kinetochores in *Xenopus* egg extracts (*8*). These studies indicate that nuclear signals, including those associated with chromosomes, influence the formation and rearrangement of microtubule structures during mitosis after NEB.

Ran-GTP, the predominant form of Ran in the nucleus (*9*), is a good candidate for such a signal (*10*–*13*). In the yeast *Saccharomyces cerevisiae*, overexpression of RanGEF1, the guanine nucleotide exchange factor for Ran, specifically suppresses a class of α-tubulin mutations that arrest with excess microtubules as large, budded cells. This suggests a link between the Ran pathway and microtubule polymerization (*12*). Moreover, cells with mutations in RanGEF1 and the Ran-binding protein, RanBP1, arrest with a mis-

Carnegie Institution of Washington, Department of Embryology, Baltimore, MD 21210, USA.

*To whom correspondence should be addressed. E-mail: zheng@mail1.ciwemb.edu

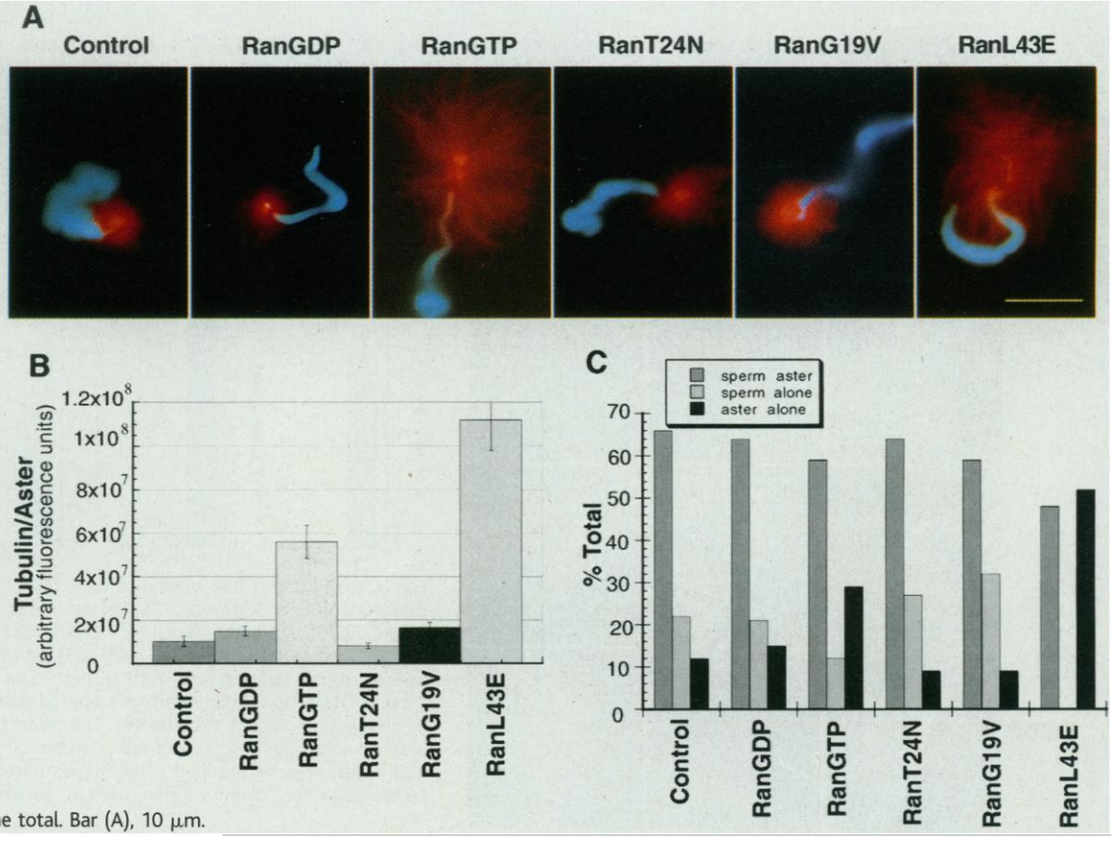

Fig. 1. The effect of Ran on microtubule aster formation by *Xenopus* sperm centrosomes in *Xenopus* egg extract. (**A**) Demembranated sperm nuclei were incubated for 7 min at room temperature in *Xenopus* egg extract containing rhodamine-labeled tubulin in the presence or absence of 25 μM GST-Ran fusion proteins. Sperm chromatin was visualized with 4′,6-diamidino-2-phenylindole (DAPI) (blue). Images were taken and manipulated (*22*) such that the microtubule intensities (red) are comparable. (**B**) Quantitation of the microtubule polymer mass in sperm asters (*22*). (**C**) The extent of microtubule aster formation induced by Ran alleles in egg extract. Each of the three classes of sperm alone, sperm with asters, and asters alone were plotted as a percentage of the total. Bar (A), 10 μm.

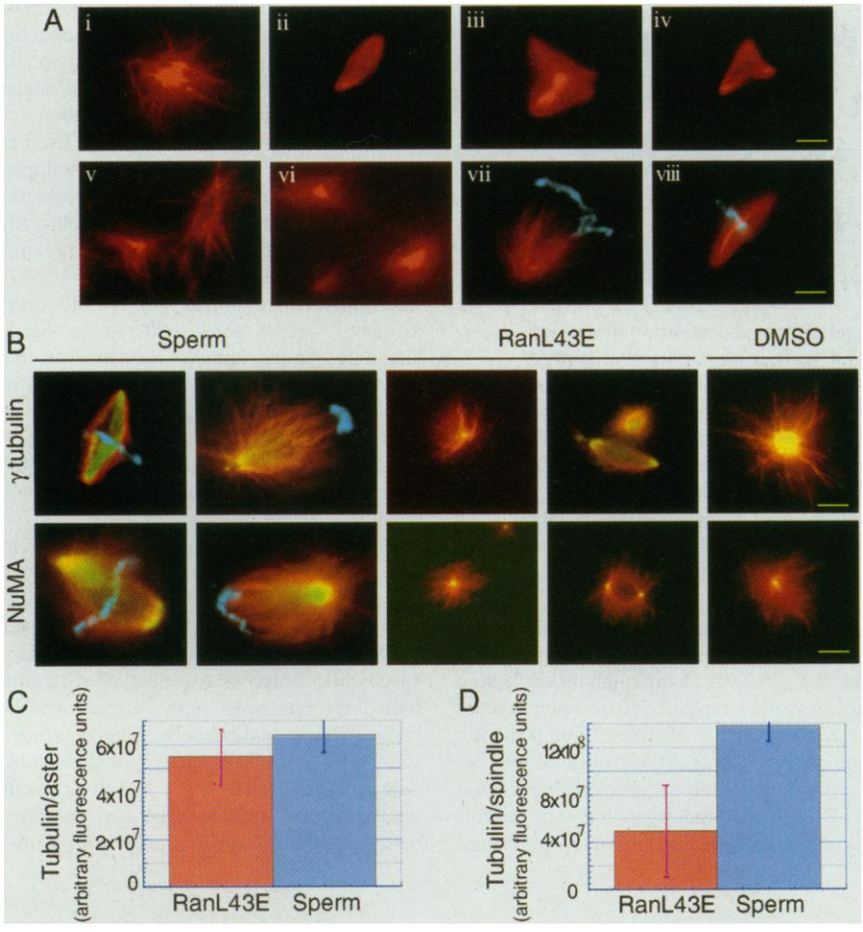

Fig. 2. Induction of microtubule aster and spindle formation in *Xenopus* egg extract. (**A**) Addition to *Xenopus* egg extract of GST-RanL43E fusion protein to 25 μM (i to iv), DMSO to 0.5% (v and vi), or demembranated *Xenopus* sperm (vii and viii) for 7 min (i and v) or 30 min (ii, iii, iv, vi, vii, and viii) at room temperature. (**B**) Immunofluorescence analysis of microtubule structures formed in *Xenopus* egg extract. Red, α-tubulin; green, γ-tubulin or NuMA; and blue, DNA (DAPI). Yellow represents the colocalization of α-tubulin and γ-tubulin or α-tubulin and NuMA. Quantification of the total microtubule polymer content of asters (**C**) or spindles (**D**), formed by sperm or RanL43E (*22*). Bar (A and B), 10 μm.

aligned mitotic spindle (*11*). In mammalian cells, a Ran-binding protein, RanBPM, is localized to the centrosome. Overexpression of RanBPM leads to the formation of ectopic microtubule asters, the centers of which contain γ-tubulin (*13*). These observations indicate that Ran could influence microtubule polymerization during mitosis.

To study the role of Ran in microtubule assembly during mitosis, we used cytostatic factor (CSF)–arrested *Xenopus* egg extract, a system used extensively to study centrosome and spindle assembly in vitro (*7*, *14*). When demembranated sperm nuclei are added to the extract, the sperm centrioles rapidly assemble into centrosomes that nucleate microtubule asters, which subsequently organize into spindles (*7*). This system allowed us to address the effect of Ran on microtubule assembly in the absence of nuclear trafficking.

To determine if Ran affects microtubule assembly from sperm centrosomes, we expressed and purified various glutathione-*S*-transferase (GST)–Ran alleles (*15*) from bacteria, then loaded them with guanine nucleotide (*16*). These proteins were added to *Xenopus* egg extracts containing demembranated sperm nuclei to a final concentration of 25 μM (the endogenous Ran concentration is ~25 μM) (*17*). Wild-type Ran-GTP, and an allele of Ran with a mutation in the effector domain, RanL43E, stimulated the formation of large microtubule asters on sperm centrosomes (Fig. 1A). The microtubule polymer mass increased 5- and 10-fold, respectively, above the control (Fig. 1B). In contrast, wild-type Ran-GDP and the Ran alleles RanT24N (a dominant negative allele predominantly bound to GDP) and RanG19V (an activated allele locked in the GTP-bound state) had little effect. The increase in microtubule polymerization activity induced by RanL43E may result from the specific mu-

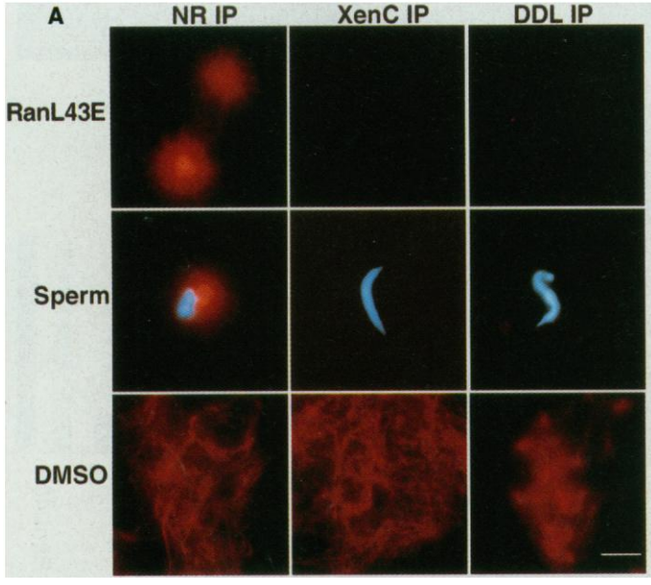

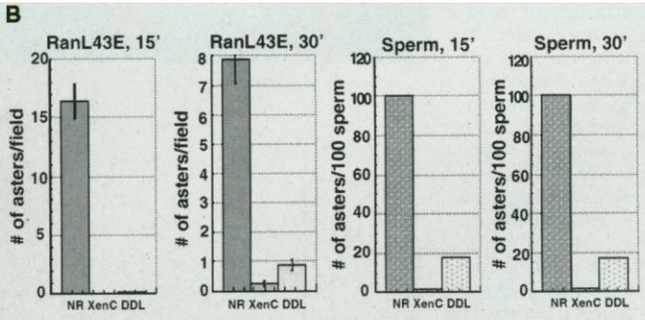

Fig. 3. Inhibition of Ran-mediated aster formation after immunodepletion of γTuRC or XMAP215. (**A**) *Xenopus* egg extract was depleted of γTuRC (with antibody XenC) or XMAP215 (with antibody DDL) or treated with rabbit random IgG (NR) (*26*), before being incubated for 15 min at room temperature with either 25 μM GST-RanL43E fusion protein, DMSO to 0.5%, or demembranated sperm nuclei in the presence of rhodamine-labeled tubulin. (**B**) The average number of RanL43E-induced asters per field, or the total number of sperm-induced asters per 100 fields, was determined after incubation of the samples at room temperature for 15 and 30 min. Bar (A), 10 μm.

tation in the effector domain (in which leucine 43 is changed to glutamic acid). This mutation not only keeps the protein in the GTP-bound active form (*15*), but could also enhance interactions with downstream effectors. RanL43E not only stimulated aster formation on all sperm, but also increased the number of asters not associated with sperm (Fig. 1C).

We next determined whether different GST-Ran alleles could induce microtubule aster formation in *Xenopus* egg extracts in the absence of sperm nuclei. Only RanL43E induced microtubule aster formation. These asters had a greater variation in size (Fig. 2C) than asters induced by sperm. However, the average microtubule mass of asters induced by RanL43E or sperm was comparable (Fig. 2C).

Taxol and dimethyl sulfoxide (DMSO) can induce microtubule aster formation in *Xenopus* egg extract by stabilizing microtubules directly (*18*, *19*). We tested whether GST-Ran fusion proteins could directly stimulate the polymerization of purified α/β-tubulin into microtubules. At concentrations of up to 65 μM, none of the Ran alleles had an effect on microtubule formation (*20*). Therefore, RanL43E must activate cellular factors in the egg extract to stimulate microtubule polymerization.

Microtubule asters formed by sperm centrosomes in CSF-arrested *Xenopus* egg extracts can polarize toward chromosomes to form monopolar and bipolar spindles (*7*). To test whether microtubule asters induced by RanL43E could rearrange into spindle-like structures, we incubated egg extracts supplemented with RanL43E for 30 min. At this time point RanL43E induced the formation of bipolar and multipolar microtubule structures that resembled mitotic spindles as well as asters (Fig. 2A). After 30 min, sperm nuclei when added to extract formed predominantly half-spindles with a few bipolar spindles (Fig. 2A). In contrast, DMSO induced only the formation of microtubule asters and disorganized arrays.

To examine whether the RanL43E spindle-like structures resembled the sperm spindles, we determined the localization of γ-tubulin and NuMA, known markers of spindle poles, by immunofluorescence (*19*, *21*). Both proteins localized to the poles of spindle-like structures induced by RanL43E- and sperm nuclei–induced spindles (Fig. 2B). Therefore, asters induced by RanL43E have the intrinsic ability to become polarized even in the absence of chromosomes. Most of the microtubule structures induced by RanL43E after 30 min were asters, varying from ~40 to 75% of the total, whereas bipolar and multipolar spindles made up between 20 to 30% and 5 to 30% of the total, respectively. No half-spindle structures were found in the RanL43E samples.

To compare directly the size and microtubule polymer mass between RanL43E and sperm spindles, we quantitated the fluorescence intensity of rhodamine-labeled tubulin in the microtubule structures produced (*22*). Bipolar spindles induced by RanL43E varied greatly in the amount of microtubule mass polymerized and contained fewer microtubules than half-spindles induced by sperm (Fig. 2D). Bipolar spindles induced by RanL43E were also smaller in size than the half-, or bipolar spindles, formed in the presence of sperm (Fig. 2). Extending the incubation time to 1 hour did not increase the size of the spindles induced by RanL43E (*20*). Although RanL43E alone can induce the formation of a bipolar spindle, centrosomes and chromosomes may be required to further stabilize and amplify the microtubule population in a spindle.

We next investigated whether RanL43E-stimulated aster formation was dependent on γTuRC, a microtubule nucleator (*23*, *24*), or XMAP215, a microtubule binding protein that promotes elongation at the plus ends of microtubules (*25*). We immunodepleted γTuRC or XMAP215 from the egg extract using the antibodies XenC (*23*, *24*) and DDL (*26*). The same amount of normal rabbit immunoglobulin G (IgG) (NR) was used as a control. Depletion of either γTuRC or XMAP215 prevented RanL43E and sperm nuclei from inducing microtubule aster formation after 15 min. However, DMSO still stimulated the production of microtubule arrays (Fig. 3A). After 30 min of incubation, RanL43E and sperm did cause the formation of some asters in γTuRC- and XMAP215-depleted extracts (Fig. 3B), but no spindles were formed. Thus, Ran-activated microtubule polymerization depends on both γTuRC and XMAP215.

The dependence of RanL43E-induced asters on γTuRC might indicate that a pericentriolar-like material is assembled. Alternatively, microtubule motors might focus the microtubules induced by RanL43E into an aster. Dynein, a minus end–directed motor, is required to focus DMSO-induced microtubules into asters as well as focused spindle poles. We therefore tested whether dynein had a role in the formation of microtubule asters induced by RanL43E using the antibody 70.1, which binds to the intermediate chain of dynein, thereby inhibiting, its activity (*19*). Antibody 70.1 was added to *Xenopus* egg extract to a final concentration of 2 mg/ml, in the presence of either DMSO, RanL43E, or sperm nuclei and its effect was compared with that of a control antibody, 9E10 (*27*). Antibody 70.1 had little effect on asters induced by sperm nuclei, but completely blocked microtubule aster formation caused by DMSO (Fig. 4A). Although antibody 70.1 prevented the formation of large microtubule asters normally induced by RanL43E, smaller groups of microtubules remained associated at one of their ends (Fig. 4A). These structures could be formed in two ways: Microtubule motors other than dynein could organize the microtubules, or small fragments of pericentriolar-like material could be formed, which then nucleates microtubules.

Ran appears to regulate microtubule structures through known cellular activators of microtubule polymerization. Ran-GTP is thought to be predominantly nuclear, thereby only coming into contact with centrosomes during mitosis after NEB occurs. Therefore, Ran could regulate microtubule structures in mitosis. This may not be surprising, because signals from the nucleus, either associated with the chromosome or closely surrounding it, are thought to be involved in stabilizing and rearranging the microtubule array during mitosis (*3*–*8*). Ran-GTP

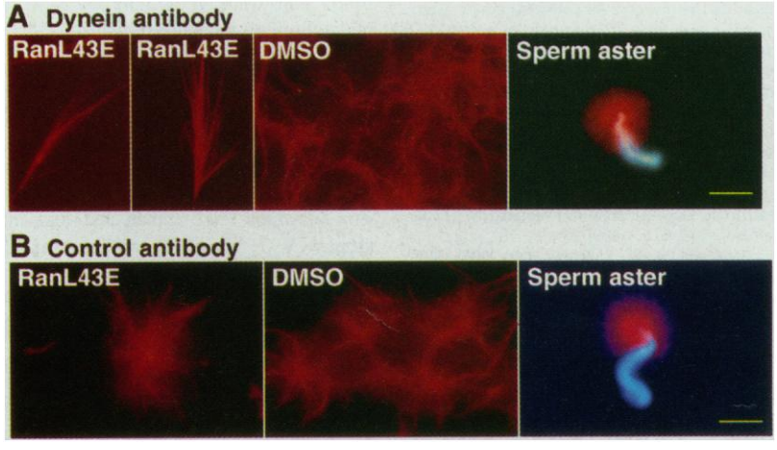

Fig. 4. The role of dynein in microtubule aster formation. (**A**) Addition of antibody 70.1, which recognizes dynein, or (**B**) antibody 9E10, which recognizes Myc, to egg extract containing rhodamine-labeled tubulin in the presence of 25 μM GST-RanL43E fusion protein, DMSO to 0.5%, or demembranated sperm nuclei. Bar (A and B), 10 μm.

may stimulate microtubule assembly through RanBPM as well as cytosolic factors such as γTuRC and XMAP215. Furthermore, Ran-GTP could act later to initiate or stabilize spindle formation. The Ran-GTPase–activating protein, RanGAP1, is localized to spindles throughout mitosis (*28*). Tethering RanGAP1 to the spindle could locally activate Ran-GTP hydrolysis to regulate spindle microtubules.

References and Notes

1. F. Verde, M. Dogterom, E. Stelzer, E. Karsenti, S. Leibler, *J. Cell Biol.* **118**, 1097 (1992).
2. F. Verde, J. Labbe, M. Doree, E. Karsenti, *Nature* **343**, 233 (1990).
3. D. Zhang and R. Nicklas, *J. Cell Biol.* **131**, 1125 (1995).
4. M. Dogterom, M. Felix, C. Guet, S. Leibler, *ibid.* **133**, 125 (1996).
5. E. Karsenti, J. Newport, R. Hubble, M. W. Kirschner, *ibid.* **98**, 1730 (1984).
6. W. Theurkauf and R. Hawley, *ibid.* **116**, 1167 (1992).
7. K. Sawin and T. Mitchison, *ibid.* **112**, 925 (1991).
8. R. Heald *et al.*, *Nature* **382**, 420 (1996).
9. M. Moore, *J. Biol. Chem.* **273**, 22857 (1998).
10. M. Dasso, *Prog. Cell Cycle Res.* **1**, 163 (1995).
11. I. Ouspenski *et al.*, *J. Biol. Chem.* **270**, 1975 (1995).
12. D. Kirkpatrick and F. Solomon, *Genetics* **137**, 381 (1994).
13. M. Nakamura *et al.*, *J. Cell Biol.* **143**, 1041 (1998).
14. A. W. Murray, *Methods Cell Biol.* **36**, 581 (1991).
15. K. Lounsbury, S. Richards, K. Carey, I. Macara, *J. Biol. Chem.* **271**, 32834 (1996).
16. M. Dasso, T. Seki, Y. Azuma, T. Ohba, T. Nishimoto, *EMBO J.* **13**, 5732 (1994).
17. GST-Ran fusion proteins were purified and loaded with guanine nucleotide as described (*16*). Each protein was concentrated to 250 μM in ultrafree centrifugal filters (Millipore), then frozen in liquid nitrogen before storage at −80°C. GST-Ran fusion proteins were diluted to 25 μM in CSF-arrested *Xenopus* egg extract for each assay. CSF-arrested *Xenopus* extracts and demembranated sperm were prepared as described (*7*, *14*). The aster formation assay used was the same as described (*24*). Samples were viewed with a Nikon Eclipse E800 microscope and images captured with a cooled charge-coupled device (CCD) camera (Princeton Instruments) with the IP labs spectrum P software.
18. K. Sawin and T. Mitchison, *Mol. Biol. Cell* **5**, 217 (1994).
19. R. Heald, R. Tournebize, A. Habermann, E. Karsenti, A. Hyman, *J. Cell Biol.* **138**, 615 (1997).
20. A. Wilde and Y. Zheng, data not shown.
21. A. Merdes, K. Ramyar, J. Vechio, D. Cleveland, *Cell* **87**, 447 (1996).
22. To quantify the microtubule polymer mass in asters or spindles, we took images with a cooled CCD camera at the same exposure and below saturation level of the camera. Fluorescence intensity of each aster or spindle was measured, and the background was subtracted from the area next to each aster or spindle with the IP labs spectrum P software. Over 30 asters or spindles were measured in each experiment.
23. Y. Zheng, M. Wong, B. Alberts, T. Mitchison, *Nature* **378**, 578 (1995).
24. O. Martin, R. Gunawardane, A. Iwamatsu, Y. Zheng, *J. Cell Biol.* **141**, 675 (1998).
25. D. L. Gard and M. W. Kirschner, *ibid.* **105**, 2203 (1987).
26. Rabbit polyclonal antibodies were raised against a peptide corresponding to the last 15 amino acids of XMAP215 (D. Gard, personal communication) and affinity-purified against the peptide (*23*). These antibodies recognize XMAP215 by immunoblotting and specifically immunoprecipitate XMAP215 in *Xenopus* egg extracts (*20*). The extent of XMAP215 depletion was over 90%, as determined by protein immunoblotting.
27. G. Evan, G. Lewis, G. Ramsay, J. Bishop, *Mol. Cell. Biol.* **5**, 3610 (1985).
28. M. Matunis, E. Coutavas, G. Blobel, *J. Cell Biol.* **135**, 1457 (1996).

29. We thank L. Zhang and O. Martin for technical support; J. Gall, C. Wiese, and Q. Guo for critical reading the manuscript; members of the Zheng lab for helpful discussion and support; I. Macara (University of Virginia, Charlottesville) and K. Lounsbury (University of Vermont) for the Ran-GST fusion proteins; A. Merdes (University of Edinburgh) for the antibody to NuMA; and D. Gard (University of Utah) for XMAP215 sequence information. Supported by NIH grant (GM56312-01) and a Pew Scholar's Award (Y.Z.).

11 March 1999; accepted 13 April 1999

Identification of a Nuclear Receptor for Bile Acids

Makoto Makishima,[1]* Arthur Y. Okamoto,[2]* Joyce J. Repa,[1]* Hua Tu,[2] R. Marc Learned,[2] Alvin Luk,[2] Mitchell V. Hull,[2] Kevin D. Lustig,[2] David J. Mangelsdorf,[1]† Bei Shan[2]

Bile acids are essential for the solubilization and transport of dietary lipids and are the major products of cholesterol catabolism. Results presented here show that bile acids are physiological ligands for the farnesoid X receptor (FXR), an orphan nuclear receptor. When bound to bile acids, FXR repressed transcription of the gene encoding cholesterol 7α-hydroxylase, which is the rate-limiting enzyme in bile acid synthesis, and activated the gene encoding intestinal bile acid–binding protein, which is a candidate bile acid transporter. These results demonstrate a mechanism by which bile acids transcriptionally regulate their biosynthesis and enterohepatic transport.

The enzymatic conversion of cholesterol to bile acids is regulated through feed-forward activation by oxysterols and feedback repression by bile acids (*1*, *2*). Because the feed-forward pathway is mediated by the liver X receptor (LXRα), a nuclear receptor that binds oxysterols (*3*), we speculated that the feedback repression pathway may also be regulated by a nuclear receptor that can bind to bile acids. The orphan receptor FXR (also called RIP14) is an ideal candidate for the bile acid receptor, because it is specifically expressed in tissues where bile acids function (such as the liver, intestine, and kidney); it is evolutionarily related to LXRα; and, like other class II nuclear receptors, it functions as a heterodimer with the retinoid X receptor (RXR) (*4*–*6*). In addition, several isoprenoid lipids can weakly activate FXR at supraphysiological concentrations; however, these compounds do not activate all species of FXR and do not bind as ligands (*4*, *7*). Thus, the identity and physiologic function of FXR ligands have remained unknown.

To test the hypothesis that FXR is the bile acid receptor, murine or human FXR expression plasmids were transfected into monkey kidney CV-1 cells or human hepatoma HepG2 cells. Cells were then treated with a series of bile acid metabolites and screened for the expression of a luciferase reporter gene. The reporter construct contained multiple copies of an inverted repeat response element (IR-1) that binds to FXR-RXR heterodimers (*4*). FXR was strongly activated by bile acids that can regulate gene expression in vivo (Fig. 1A) (*8*, *9*). The activation of FXR was specific and limited to the primary bile acid chenodeoxycholic acid (CDCA) and to a much lesser extent to the secondary bile acids deoxycholic acid (DCA) and lithocholic acid (LCA) (Fig. 1, A through C). Other closely related compounds such as cholesterol, oxysterols, steroid hormones, and other bile acid metabolites were inactive in this assay at concentrations up to 100 μM (Fig. 1) (*10*). The most potent activator, CDCA, had a half-maximal effective concentration (EC_{50}) of 50 μM and 10 μM on murine and human FXR, respectively (Fig. 1B). These concentrations are well within the physiologic intracellular range reported in vivo (*11*). In addition, FXR was the only protein activated by bile acids (Fig. 1C). These results suggest that bile acids are the physiologic ligands of FXR.

After binding to ligand, nuclear receptors undergo a conformational change that increases their affinity for coactivator proteins such as SRC-1, a key step in the assembly of an active transcription complex (*12*). To further demonstrate that bile acids are physiologic ligands for FXR, a mammalian two-hybrid assay (*13*) was used to probe for a functional interaction in vivo between the FXR ligand-binding domain (LBD) and SRC-1. In transfected HEK-293 kidney cells, CDCA treatment promoted the association of FXR LBD and SRC-1 as expected (Fig. 1D). The EC_{50} of this response (20 μM) is similar to that for CDCA-induced transactivation of FXR (Fig. 1B).

The receptor-interacting domain of the co-

[1]Howard Hughes Medical Institute and Department of Pharmacology, University of Texas Southwestern Medical Center, 5323 Harry Hines Boulevard, Dallas, TX 75235–9050, USA. [2]Tularik Incorporated, Two Corporate Drive, South San Francisco, CA 94080, USA.

*These authors contributed equally to this work.
†To whom correspondence should be addressed. E-mail: davo.mango@email.swmed.edu